The model squid–vibrio symbiosis provides a window into the impact of strain- and species-level differences during the initial stages of symbiont engagement

Sabrina Koehler,[1][†] Roxane Gaedeke,[1]
Cecilia Thompson,[2] Clotilde Bongrand,[1] Karen L. Visick,[2]
Edward Ruby[1] and Margaret McFall-Ngai [1]*
[1]Pacific Biosciences Research Center, University of
Hawaii at Manoa, Honolulu, Hawaii, USA.
[2]Department of Microbiology and Immunology,
Loyola University Chicago, Chicago, Illinois, USA.

Summary

Among horizontally acquired symbioses, the mechanisms underlying microbial strain- and species-level specificity remain poorly understood. Here, confocal-microscopy analyses and genetic manipulation of the squid–vibrio association revealed quantitative differences in a symbiont's capacity to interact with the host during initial engagement. Specifically, dominant strains of *Vibrio fischeri*, 'D-type', previously named for their dominant, single-strain colonization of the squid's bioluminescent organ, were compared with 'S-type', or 'sharing', strains, which can co-colonize the organ. These D-type strains typically: (i) formed aggregations of 100s–1000s of cells on the light-organ surface, up to 3 orders of magnitude larger than those of S-type strains; (ii) showed dominance in co-aggregation experiments, independent of inoculum size or strain proportion; (iii) perturbed larger areas of the organ's ciliated surface; and, (iv) appeared at the pore of the organ approximately 4×s more quickly than S-type strains. At least in part, genes responsible for biofilm synthesis control the hyperaggregation phenotype of a D-type strain. Other marine vibrios produced relatively small aggregations, while an array of marine Gram-positive and -negative species outside of the Vibrionaceae did not attach to the organ's surface. These studies provide insight into the impact of strain variation on early events leading to establishment of an environmentally acquired symbiosis.

Introduction

Many organisms acquire their symbiotic partners from the surrounding environment each generation, that is, by horizontal transmission (McFall-Ngai, 1998; Bright and Bulgheresi, 2010; Salem *et al*., 2015; Cao and Goodrich-Blair, 2017). Unlike vertical transmission, in which provision of the symbiont cells in or on the host's eggs assures specificity, symbiont selection in environmentally acquired partnerships usually occurs against an abundance of non-specific microbes in the host habitat. This mode of acquisition is best understood in terrestrial animals, such as insects (Aanen *et al*., 2002; Mueller *et al*., 2015; Powell *et al*., 2016; Takashita and Kikuchi, 2017), where transfer of symbionts relies on direct interactions of the juveniles with infected conspecifics. In aquatic habitats, which can support a protracted free-living stage of the microbial partner, the mechanisms by which symbioses are established with fidelity each generation are largely undescribed. Typically, the potential symbiont cells represent only a fraction of the ambient environmental microbes, and efforts to observe the stochastic, initial interactions of these cells with host tissues over time and space face a formidable challenge.

Horizontal transmission also impacts the genetic features of the symbiont cells. For example, in model associations, such as the legume–rhizobia symbioses, specificity can be influenced by antagonistic interactions

occurring between different combinations of host and symbiont genotypes, or between strains of the same symbiont species within a given host (Pellmyr and Huth, 1994; Frank, 1996; Kiers *et al*., 2003; Sachs *et al*., 2004, Poulsen and Boomsma, 2005; Bongrand *et al*., 2016). A recent study of the model symbiosis between *Steinernema* nematodes and *Xenorhabdus bovienii* (Murfin *et al*., 2015) showed that strain-level differences in the fitness benefits of microbial symbionts drive variation in the success of host–microbe associations, likely contributing to the maintenance of symbiotic associations over evolutionary time. In contrast, within the human gut microbiota, most bacterial species are represented by multiple cocolonizing strains (Caro-Quintero and Ochman, 2015; Greenblum *et al*., 2015; Noecker *et al*., 2017), although where they occur relative to one another, how such diversity is achieved and maintained, and whether strain diversity impacts metabolic function or host health, are questions that remain largely unanswered.

The association between the Hawaiian bobtail squid, *Euprymna scolopes*, and the luminous bacterium *Vibrio fischeri* has been studied for more than 25 years as an experimental model for the establishment, development and maintenance of horizontally transmitted symbioses (McFall-Ngai and Ruby, 1991, Nyholm and McFall-Ngai, 2004, McFall-Ngai, 2014). Females typically lay clutches of 100–400 eggs, a feature that enhances the statistical power of colonization experiments. During embryogenesis in the egg, the host develops a nascent organ poised to interact with symbionts upon hatching. The symbiosis, which is strictly specific for *V. fischeri* (McFall-Ngai and Ruby, 1991), is established within hours after the juvenile squid emerges from the egg. Species specificity is determined by both the biomechanical and biochemical landscape presented by the surface of the juvenile light organ. Briefly, two complex sets of ciliated epithelia, one on each lateral face of the hatchling organ, produce flow fields that entrain 2-μm particles (e.g., bacterial cells) into a region near pores (Nawroth *et al*., 2017), through which the symbionts enter the host tissues. Each of the superficial epithelial regions consists of cells with long, metachronally-beating cilia that populate the pairs of anterior and posterior 'appendages' on either side of the organ (Fig. 1), as well as a set of short cilia that surround and expand outward from the pores (Nawroth *et al*., 2017). The entrained particles associate with mucus, which contains antimicrobial compounds (e.g., NO, lysozyme, peptidoglycan-recognition proteins, and lipopolysaccharide-binding proteins; (McFall-Ngai, 2014)) that have been shed from the organ's ciliated surface. The induction of mucus secretion is a nonspecific response to exposure to peptidoglycan released by environmental Gram-negative and Gram-positive bacteria (Nyholm *et al*., 2000, 2002).

Early studies of the process of symbiont initiation showed that several species of Gram-negative, but not Gram-positive, bacteria would aggregate within this mucus (Nyholm *et al*., 2000). The symbionts attach to host cilia (Altura *et al*., 2013), inducing a change in host gene expression that results in an increase in antimicrobials in the environment that are at higher concentrations in the host tissues into which the symbionts migrate (Kremer *et al*., 2013). This modification of the host microenvironment occurs during the first 1–3 h, when *V. fischeri* cells slowly aggregate and become the sole phylotype in the aggregations, suggesting that a biochemical environment is created that both favours association with the specific symbiont, and primes it for transit into antimicrobial-rich host tissues (Kremer *et al*., 2013). Once aggregated on the surface, the symbiont cells pass through the pores and proceed along a ~100-μm journey into the crypts (Fig. 1). On average, a single *V. fischeri* cell enters each of the 6 crypts (Dunn *et al*., 2006; Wollenberg and Ruby, 2009), where they grow to a total symbiont population of 10^5–10^6 cells (Ruby and Asato, 1993). Even in the absence of *V. fischeri*, no other bacterial phylotypes in the host's environment are capable of entering host tissues beyond the pore region (Nyholm *et al*., 2000).

The majority of studies of this initiation process has been carried out using the *V. fischeri* symbiont strain ES114 (Boettcher and Ruby, 1990), in which genetic and genomic tools were first developed. Using this strain, the nascent symbiont has been shown to play a direct role in the aggregation process. For example, the regulator RscS is a critical factor for biofilm formation and subsequent colonization of host tissues by strain ES114 (Visick, 2009). RscS is a sensor kinase that responds to environmental conditions and enhances biofilm formation by inducing the transcription of a locus of symbiosis polysaccharide (*syp*) genes (Yip *et al*., 2005, 2006). A severe colonization defect results from the lack of either the *rscS* gene (Visick and Skoufos, 2001; Mandel *et al*., 2009), or the cluster of *syp* genes it controls (Yip *et al*., 2005; Shibata *et al*., 2012). Taken together, the data described above indicate that both the host and the symbiont contribute factors and activities that drive the initiation of a successful association.

Recent studies of the system have demonstrated that the symbiotic population in a naturally occurring *E. scolopes* is not clonal but, instead, contains several phenotypically and genomicly distinguishable strains of *V. fischeri* (Wollenberg and Ruby, 2009, 2012; Bongrand *et al*., 2016). In experiments where host-colonization potential was examined when strains were competed against one another, two phenotypes were noted: (i) a dominant (D-type) behaviour, in which the host organ was usually colonized by a single strain; and, (ii) a
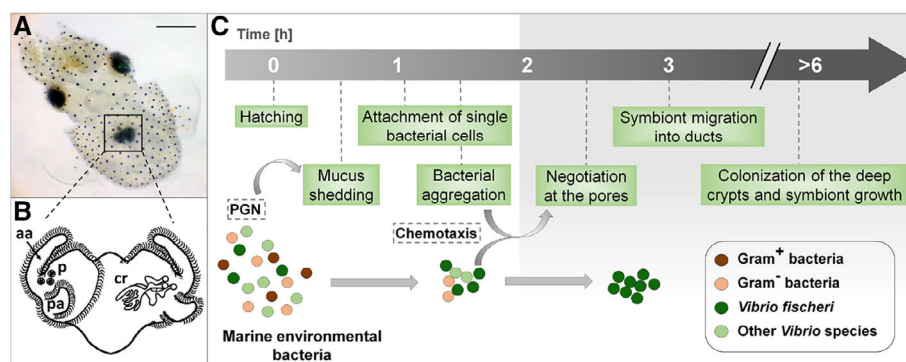
Fig. 1. The onset of the squid–vibrio symbiosis. A. A newly hatched Hawaiian bobtail squid, *Euprymna scolopes*, with its bioluminescent light organ (black square) in the centre of the body cavity; scale bar = 500 μm. B. An illustration of the external (left side) and internal (right side) features of the nascent organ, as viewed ventrally: aa, anterior appendage; cr, crypts; p, pores; pa, posterior appendage. C. Events in the recruitment of the specific symbiont, *Vibrio fischeri*, into the organ's crypts, depicting the stages at which selectivity occurs. The grey shading (right) shows the internal portions of the organ, regions specific to *V. fischeri*. PGN, peptidoglycan released from bacteria in the ambient seawater. [Color figure can be viewed at wileyonlinelibrary.com]

sharing (S-type) behaviour, in which more than one strain would co-colonize the same animal (Bongrand *et al.*, 2016). The variation in the D- and S-type strains in their ability to dominate or co-colonize the crypts under these experimental conditions revealed a dominance hierarchy among these strains. Genomic analysis revealed that the D-strains are a recently diverged clade of *V. fischeri* (Bongrand *et al.*, 2016). These phenotypic and genotypic differences among *V. fischeri* strains render the squid–vibrio association an exceptional model system to study the impact of symbiont diversity on initiation, maintenance and persistence of host–microbe interactions.

In this study, we used the ability to view initial events of host–symbiont interaction directly and in real time to examine the impact of *V. fischeri* strain variation on initiation of the squid–vibrio symbiosis. The data provide evidence that strain variation is a major determinant of symbiosis initiation, affecting the very first interactions of the symbiont with host tissues. Genetic analyses suggested that strain variability in symbiosis initiation is controlled, at least in part, by differences in the relative level of a strain's biofilm formation. In addition, we explored the capacity of environmental bacteria, including other

Vibrio species, to interact with host tissues. The ability to form aggregates on the juvenile light organ surface was restricted to the Vibrionaceae tested. This study illustrates the wide range of intraspecies and interspecies variation that can occur in the initial interactions between a host and environmental bacteria during the minutes to hours surrounding the first encounter with the ambient environment, and underscores the impact of strain variation on symbiosis.

Results and discussion

V. fischeri *strains exhibit differences in the extent of association with host cells during their initial recruitment into symbiosis*

We examined the aggregation behaviour of 8 *V. fischeri* strains, including 4 'niche-dominant' (D) and 4 'niche-sharing' (S) isolates (Table 1) from *E. scolopes* light organs. The D-type strains associated with the light organ (i.e., appeared at the pores, and aggregated) more quickly, in higher numbers, and across a larger area of the juvenile's organ surface (Table 1). The D-type

Table 1. Aggregation characteristics of D- and S-type *V. fischeri* symbiont strains

Strain name[a]	N[b]	Average number of cells, cells in aggregate (range)[c]	Approximately time to form an aggregate (min)[d]
MB13B2	27	20 000 (41–85 000)	10–15
KB2B1	23	2400 (18–16 000)	10–15
MB11B1	29	310 (3–3900)	30
MB13B3	26	300 (2–2900)	60
MB13B1	23	110 (6–550)	60
ES114	24	41 (1–200)	60
MB15A4	24	32 (1–130)	60
MB15A5	21	79 (1–750)	60

[a]Strains above the dashed line are D-type.
[b]Number of animals analysed; inoculated with 10^5 CFU ml^{-1} seawater for 3 h.
[c]Approximate number of cells in the aggregate (see *Experimental procedures* for details).
[d]Time after inoculation at which the first evidence of aggregated cells was observed.

V. fischeri strains, MB13B2, KB2B1 and MB11B1, formed bacterial aggregations 1–3 orders of magnitude larger than all of the other strains, with MB13B2 having, on average, the largest aggregations (Fig. 2A and B). In addition, strains MB13B2 and KB2B1 formed aggregations as early as 10–15 min post-inoculation (Table 1), about four times faster than the well-studied S-type strain, *V. fischeri* ES114. The *V. fischeri* strains MB13B3 and MB13B1 showed no significant difference in size or time of aggregation, although they group with the D- and S-type strains respectively. Similarly, the remaining S-type *V. fischeri* strains showed no significant difference in aggregation size or timing across strains (Fig. 2B). Based on these data, we established a ranking of these eight strains in their ability to form bacterial aggregations on the surface of the host light organ as following:

MB13B2 > KB2B1 > MB11B1 > MB13B3 = MB13B1 > ES114 = MB15A4 = MB15A5 (Fig. 2B).

To investigate the dynamics of aggregation in detail, we focused on one *V. fischeri* D-type strain, MB13B2, and one S-type strain, ES114. First, cohorts of animals were exposed to each strain at one of three concentrations: 10^3, 10^4 or 10^5 CFU ml^{-1} of seawater. The lower cell density (10^3 CFU ml^{-1}) approximates the reported abundance of *V. fischeri* cells that the squid host might encounter in its natural habitat (Jones *et al*., 2007) and, thus, provides insight into the aggregation behaviour of these strains under typical environmental conditions. Similar to our results for initial strain comparisons (Fig. 2B), the D-type *V. fischeri* strain, MB13B2, formed significantly larger aggregations, under both naturally occurring and enriched bacterial concentrations, than the S-type strain, ES114 (Fig. 2C).
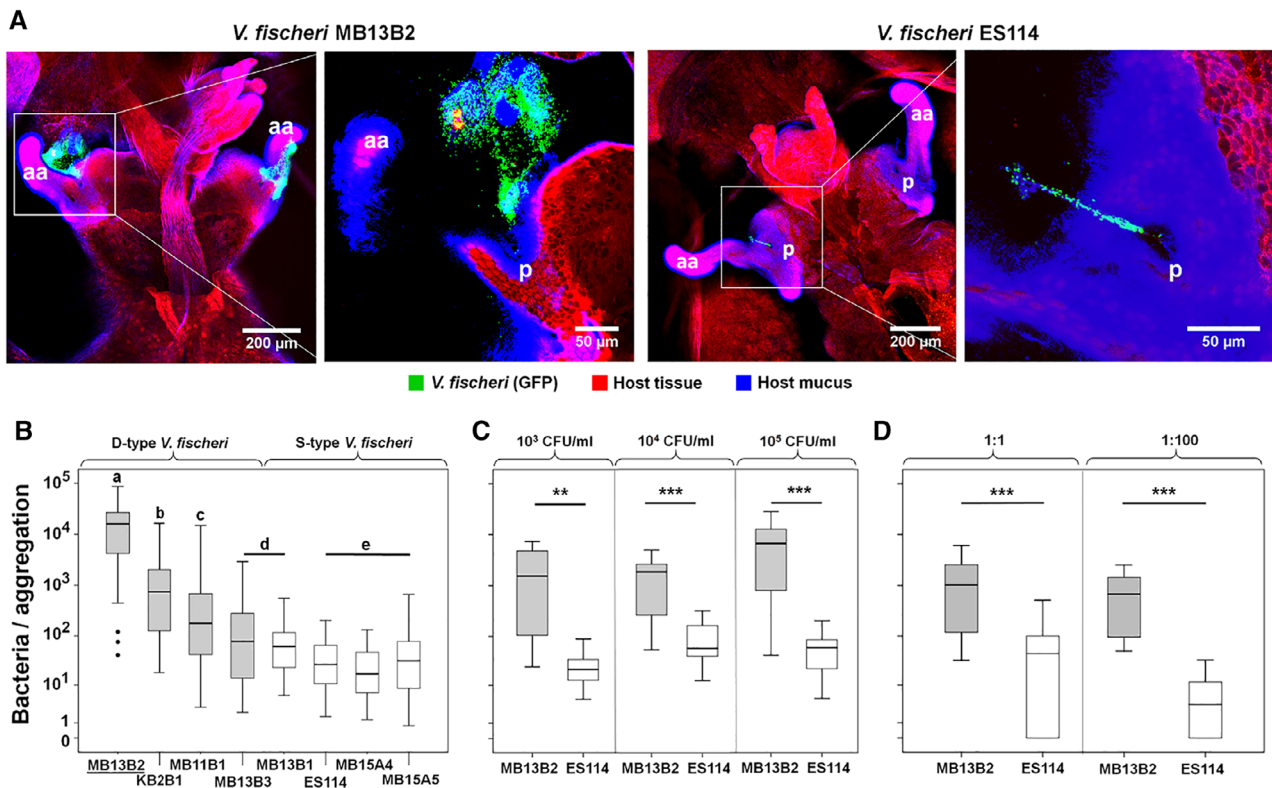

Fig. 2. Differences in aggregation behaviour between strains of *V. fischeri*. A. Two pairs of high and low magnification confocal-microscopy images illustrating the difference in the extent of bacterial aggregation on the surface of the squid's light organ. Images captured at 3 h post-inoculation with GFP-expressing cells of either the *V. fischeri* D-type strain MB13B2 (left) or S-type strain ES114 (right); aa, anterior appendage; p, pores. Red, Cell Tracker Orange; blue, WGA (wheat-germ agglutinin) Alexa 633. B. D-type *V. fischeri* strains generally had higher maxima as well as a large variation in average aggregation size; Kruskal–Wallis Test: Chi^2 = 192, *df* = 7, *p* < 0.001 (for *N* values, see Table 1); the letters above the columns signify that those values are statistically significantly different from columns with another letter; bold horizontal lines represent medians; boxes comprise the interquartile ranges; bars indicate minimum and maximum values. C. The size of aggregates produced by MB13B2 and ES114 cells was independent of the inoculum concentration; left panel, 10^3 CFU ml^{-1}, Mann–Whitney *U* = 7, *Z* = −3.13, *p* = 0.002 (**); middle panel, 10^4 CFU ml^{-1}, Mann–Whitney *U* = 20, *Z* = −3.24, *p* = 0.001 (***); right panel, 10^5 CFU ml^{-1}, Mann–Whitney *U* = 10, *Z* = −3.56, *p* < 0.001 (***); *N* > 5 for all treatments. D. The relative aggregation effectiveness of MB13B2 and ES114 cells was independent of the co-inoculum ratio; left panel, ratio 1:1 = 10^3 CFU ml^{-1} each strain, Wilcoxon-signed-ranks test: *Z* = −4.11, *n* = 22, *p* < 0.001 (***); right panel, ratio 1:100 = 10^3 CFU ml^{-1} MB13B2 and 10^5 CFU ml^{-1} ES114: Wilcoxon-signed-ranks test: *Z* = − 3.41, *n* = 15, *p* = 0.001 (***). Shaded boxes = D-type strains. [Color figure can be viewed at wileyonlinelibrary.com]

To determine the effect of co-inoculation on the patterns of aggregation, strains MB13B2 and ES114 were co-inoculated at ratios of 1:1 and 1:100. As expected, at a 1:1 inoculum (10^3 CFU of each strain per ml), strain MB13B2 outcompeted strain ES114. However, even when the concentration of ES114 was increased 100-fold in the inoculum (i.e., 10^5 CFU ml^{-1}), this strain comprised less than 1% of the bacteria appearing in the aggregates, which consisted principally of MB13B2 cells (Fig. 2D; Supporting Information Fig. S1). Thus, the combined results indicate that the superiority of the D-type strain MB13B2 for aggregation on the organ surface was largely independent of both the initial bacterial density, and the relative abundance of D- and S-type strains that the host encounters during symbiosis initiation.

How might strains that form larger aggregations have a colonization advantage over those forming smaller ones (Bongrand *et al*., 2016)? One possible benefit would be the dilution of host-derived antimicrobials (McFall-Ngai, 2014) within the large, biofilm-rich (see below) aggregations; a second might be that these strains, unlike ES114, reach the pore sooner (Table 1) and are already 'primed' for successful navigation of the journey to the crypts (Wang *et al*., 2010; Kremer *et al*., 2013). In any case, the advantage, while uniform within the D-strains, is not directly proportional to their aggregate size (Fig. 2), or to the ratio of strains within the aggregate (Supporting Information Fig. S1) (Bongrand *et al*., 2016).

Many studies have demonstrated that differences between strains of a pathogenic species are reflected in their various levels of persistence and host responses (for review, see Palmer and Brayton, 2013). In addition, several studies have reported on the impact of strain variation in mutualistic symbioses, including the *Steindernema-Xenorhabdus* association (Murfin *et al*., 2015; McMullen *et al*., 2017) and in the plant-rhizobium interactions (Heath and Tiffin, 2007; Ezzakkioui *et al*., 2015; Bastone *et al*., 2017). In contrast, to the authors' knowledge, few, if any, data are available on the differential behaviour of a series of strains of a beneficial microbe during the initial minutes to hours of an animal–host association. For instance, while metagenomics have enabled descriptions of high levels of strain diversity within the mammalian gut microbiome (Greenblum *et al*., 2015; Ellegaard and Engel, 2016), the complexity of these communities has made understanding strain-level dynamics a challenging goal. Studies of binary associations, such as the squid–vibrio system and the nematode–*Xenorhabdus* association (Goodrich-Blair, 2007), as well as simple microbial consortia, such as those of the hydra (Deines *et al*., 2017), leech (Graf *et al*., 2006) and honeybee (Kwong and Moran, 2016), are offering opportunities for extensive experimental manipulation of strain variation. These invertebrate models promise to provide insight into the rules governing when, where and how strain-level variation is a significant factor in maintaining healthy, robust, symbiotic communities.

Aggregation of bacteria on the light organ surface perturbs the ultrastructure of the cilia, an effect whose extent reflects the aggregate size

To determine how the host-cell surface responds to aggregating bacteria during initiation of symbiosis, we examined the interaction of different bacteria with the light organ's ciliated field by both transmission electron microscopy (TEM) and confocal microscopy. A distinct structural modification of the cilia tips was observed when host cells were in association with *V. fischeri* cells (Fig. 3), independent of strain type. Such structurally altered cilia appeared exclusively in areas where bacteria were directly interacting with the ciliated surface; because the cells of a hyperaggregating strain are more abundant, the perturbations were more extensive. Aposymbiotic animals typically had only a few such modified cilia randomly distributed (Fig. 3E and F). Interestingly, this perturbation also occurred with *V. campbellii* strain KNH1, a bacterium that forms aggregates (Nyholm *et al*., 2000) but is unable to colonize the light organ.

The aposymbiotic data suggest that a few environmental cells capable of causing this perturbation were present in the ambient seawater, because the effect was not detected in animals exposed to bacteria-free filtered seawater (0.2 μ pore-size). Filtering does not remove soluble bacterial microbe-associated molecular patterns (MAMPs), such as lipopolysaccharide (LPS) and peptidoglycan derivatives that are known signalling molecules in the squid–vibrio system (McFall-Ngai *et al*., 2010), indicating that these bioactive soluble signals are not responsible for cilia-tip distortion. Because similar distortions can be an artefact of sample preparation (Short and Tamm, 1991), we confirmed this phenotype by live imaging both aposymbiotic and symbiotic animals, anaesthetised either by cooling or with 2% ethanol.

The mechanisms mediating the perturbation of ciliary tips, as well as the functional significance of this ultrastructural modification, remain to be determined; however, similar modifications of cilia have been previously reported (i) in several marine invertebrate tissues (for review, see Deiner *et al*., 1993), and (ii) as a result of genetic defects in cilia biogenesis and maintenance (Siller *et al*., 2015). A possible cause of such distortion on the light organ's ciliary surface could be a biomechanical consequence of the direct interaction of bacteria with the tip of the cilia (Nawroth *et al*., 2017). Specifically, the swelling and coiling of ciliary tips into paddle-like structures could result from changes in membrane tensile
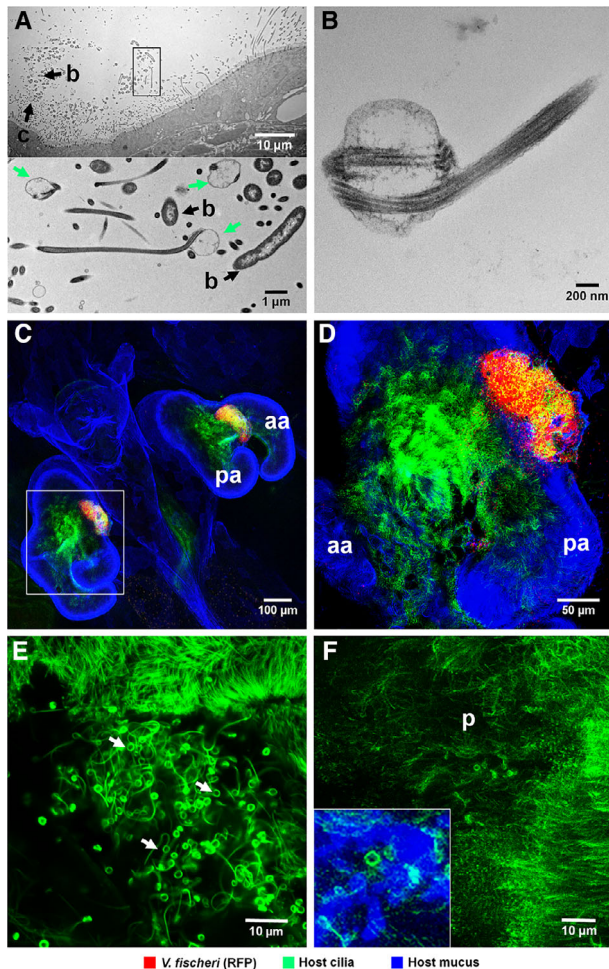
Fig. 3. Association of *V. fischeri* cells with cilia on the surface of the light organ. A, B. TEM images of cells of *V. fischeri* strain MB13B2, demonstrating structurally altered cilia in areas where bacteria directly interact with the ciliated surface of the light organ. (A) *Upper panel*: low magnification, showing the relationship of aggregating *V. fischeri* cells to the host's ciliated epithelium; b, bacteria; c, structurally altered cilia. *Lower panel*: boxed area (rotated 90° clockwise) at higher magnification; altered cilia with swollen, paddle-shaped tips (green arrows) in association with *V. fischeri* cells. (B) High-magnification image, showing typical features of distorted cilia tip. C–E. Confocal images at increasing magnification reveal host-cilia interactions with MB13B2 cells. (C) Low magnification, showing whole light organ. (D) Three-fold higher magnification of boxed area in C, showing aggregating bacteria. Yellow area indicates the co-localization of cilia (green) and *V. fischeri* cells (red). (E) Five-fold higher magnification than D, with only the green laser channel active to show the structurally altered cilia (green threads with terminal paddles) that form in areas of bacterial association (white arrows). The upper sector of this image shows structurally unaltered cilia for comparison. F. High-magnification confocal image of the ciliated surface of an aposymbiotic animal, where only an occasional cilium has an altered tip (inset, lower left); aa, anterior appendage; pa, posterior appendage; p, pore. Green, Tubulin Tracker; blue, WGA (wheat-germ agglutinin) Alexa 633. [Color figure can be viewed at wileyonlinelibrary.com]

stress on the elastic axonemes of the cilia (Deiner *et al.*, 1993), a force that may occur when motile *V. fischeri* cells attach to the cilia.

Studies of ES114 showed that, during first encounter of the partners, as few as 5 cells attaching to the short cilia on the light organ surface are sufficient to signal changes in host gene expression (Kremer *et al.*, 2013; Nawroth *et al.*, 2017), likely through the presentation of MAMPs like peptidoglycan and LPS (McFall-Ngai *et al.*, 2010). The greater surface area covered by hyperaggregating strains, and their earlier appearance at the pores, predict that these strains may signal the host's ciliated cells more strongly and quickly.

The hyperaggregating behaviour of a V. fischeri D-type strain is regulated by genes required for biofilm formation in an S-type strain

Studies of the S-type strain ES114 have demonstrated that genes for Syp-biofilm formation are essential for light-organ aggregation and colonization by *V. fischeri* (Yip *et al.*, 2005, 2006, Shibata *et al.*, 2012). To investigate whether these genes are required for the hyperaggregation of a D-type strain, we generated two mutations in *V. fischeri* strain MB13B2: (i) Δ*rscS*, defective for the Syp-biofilm positive regulator RscS, and (ii) Δ*sypQ*, missing a glycosyltransferase required for Syp-biofilm formation. Squid were inoculated with these strains at a concentration of 10^3 CFU ml^{-1} to mimic conditions that they might encounter in their natural environment. The Δ*rscS* mutation resulted in a statistically significant few-fold reduction in the number of cells amassed; however, the aggregate was still unexpectedly large (Fig. 4). In contrast, for most (> 80%) squid inoculated with the strain with a *sypQ* deletion, no bacterial aggregations were observed at the light organ surface; similarly, those few aggregates that had formed were approximately 1000-fold reduced in the size, to a level characteristic of S-type strains (Table 1). Genetic complementation of the *sypQ* mutation restored the aggregation phenotype to that of the parental MB13B2 strain (Fig. 4).

The ability of most of the D-type strains to form symbiotic aggregates that were larger than those of ES114 suggested that these strains would also produce an extensive biofilm outside of the host. Thus, we assessed the ability of MB13B2, the D-type strain with the most extreme hyperaggregation phenotype, to form biofilms in two distinct assays, (i) wrinkled colony formation on solid agar media, and (ii) pellicle formation in static liquid cultures. The S-type strain ES114 is unable to form biofilms under either of those conditions, and so was used as a negative control, while KV4366 (*rscS***), a previously described (Marsden *et al.*, 2017), constitutively RscS-induced mutant of ES114 (Supporting Information Table S1), was used as a positive control.

On agar plates, the *rscS***, biofilm-overproducing strain formed robust, cohesive, wrinkled colonies (Fig. 5A). In

Fig. 4. Role of bacterial biofilm-formation genes in a hyperaggregating strain. *Left panel*: Genetic manipulation of strain MB13B2 by deletion of the gene encoding RscS, a positive regulator of Syp-biofilm formation, only partially reduces the level of bacterial aggregation as compared with its wild-type parent. In contrast, a deletion of an essential Syp structural gene (*sypQ*) almost completely eliminated the aggregating phenotype of MB13B2 (Kruskal–Wallis Test: Chi^2 = 20.6, *df* = 3, *p* < 0.001). The defect could be complemented by carriage of a wild-type copy of *sypQ*, *in trans*, on pMKF15 (Supporting Information Table S2), but not the vector (pKV282) alone. The letters above the columns signify that those values are statistically significantly different from columns with another letter; bold horizontal lines represent medians, boxes in this plot comprise the interquartile ranges (IQR); bars indicate 1.5 IQR of the data shown. The dots represent outliers. *Right panel*: confocal images showing the aggregation of mutants compared with the wild-type parent, *V. fischeri* strain MB13B2. aa, anterior appendage; pa, posterior appendage; p, pores. Red, Cell Tracker Orange; blue, WGA (wheat-germ agglutinin) Alexa 633. [Color figure can be viewed at wileyonlinelibrary.com]
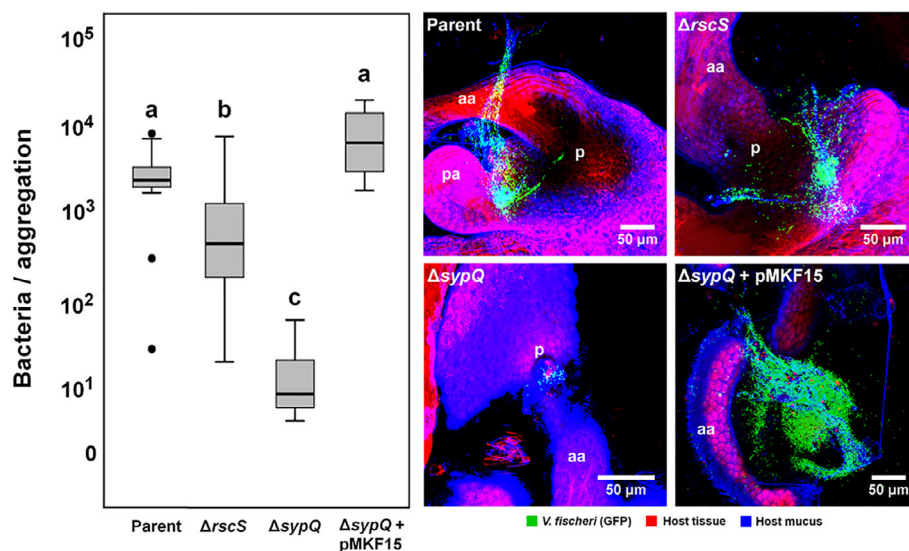
contrast, MB13B2 did not form colonies with either the surface architecture or cohesion of induced biofilms and, as expected, both the *sypQ* and *rscS* mutant derivatives of this strain also exhibited the smooth phenotype, similar to colonies of the negative control strain. Consistent with its increased symbiotic aggregation phenotype, however,

MB13B2 formed an extensive pellicle in static liquid culture following prolonged incubation (i.e., 10 days) at room temperature. While the ES114 culture formed a thin pellicle over that time period, it could be readily resuspended into a turbid culture (Fig. 5B, i). However, MB13B2 formed a thick pellicle at the air/liquid interface, similar to
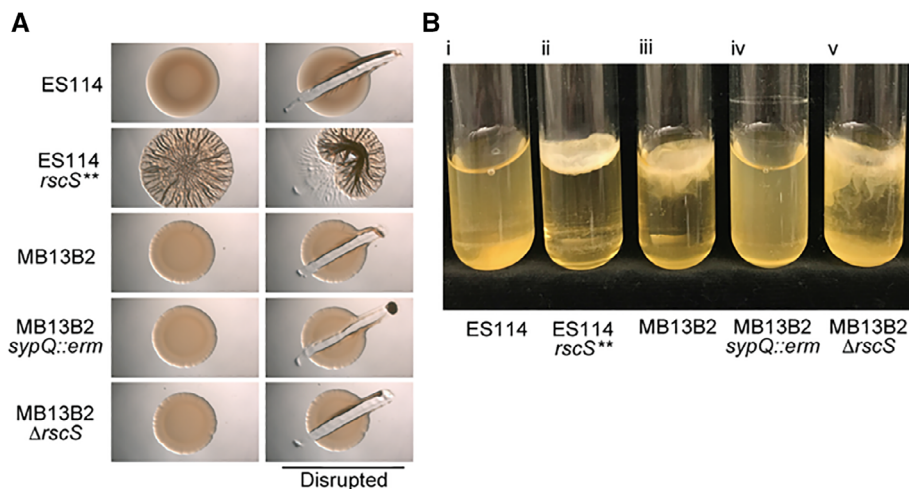

Fig. 5. *In vitro* biofilm phenotypes. A. Development of a wrinkled-colony morphology. Ten microliters of a culture of each of five *V. fischeri* strains were spotted onto LBS agar plates. After 72 h of growth at 24°C, colonies were disrupted with a toothpick to assess colony cohesiveness, which is an indicator of Syp-encoded polysaccharide production (Yip *et al.*, 2005, 2006). B. Pellicle formation in static liquid culture. Five strains of *V. fischeri* [(i) ES114, (ii) ES114 *rscS*** (KV4366), (iii) MB13B2, (iv) MB13B2 Δ*sypQ* (KV8195), and (v) MB13B2 Δ*rscS* (CBNR107)] were inoculated into 5 ml of LBS broth, and grown to log phase under shaking conditions. Cultures were then incubated statically at 24°C for 10 days, and assessed for the presence of a surface pellicle. [Color figure can be viewed at wileyonlinelibrary.com]

the biofilm-overproducing strain (Fig. 5B, ii and iii). These pellicles were robust, as manually shaking the culture dislodged the pellicle from the surface, but did not resuspend the cells as a turbid culture. Mutation of *sypQ* completely eliminated pellicle formation by strain MB13B2, indicating that this D-type strain forms *syp*-dependent biofilms under these conditions (Fig. 5B, iv). These data thus reveal that the D-type strain MB13B2 has an enhanced ability to form *syp*-dependent biofilms, relative to ES114, a result that correlates with its hyper-aggregation during symbiosis initiation. Why MB13B2 responds differently in liquid culture and solid agar media by forming biofilms only in the former environment remains to be determined, but these data suggest that the liquid assay is more reflective of the fluid conditions of the symbiotic interaction.

In contrast to Δ*sypQ*, the *rscS* mutant retained the ability to form a robust pellicle that could be dislodged from the surface but not resuspended (Fig. 5B-v). These findings suggest that other regulatory inputs, in addition to RscS, control the hyperproduction of a *syp*-dependent biofilm by MB13B2. Indeed, in *V. fischeri* strain ES114, SypF is a required sensor kinase that activates biofilm formation and symbiotic colonization (Visick, 2009; Norsworthy and Visick, 2015), as does HahK, which, like RscS, activates via SypF (Tischler *et al*., 2018). In contrast, BinK, which functions independently of RscS, directly inhibits *syp*-biofilm formation (Brooks and Mandel 2016). It is possible that SypF, HahK and/or BinK, all of which are encoded by MB13B2 (Bongrand *et al*., 2016) and share greater than 99% amino-acid identity with their homologues in strain ES114, play a more important role in regulating biofilm formation in MB13B2. Another plausible explanation includes the upregulation of an additional biofilm component whose activity depends on the Syp polysaccharide; that is, biofilms formed by other species involve outer membrane vesicles, extracellular DNA and proteins. Some of these factors are involved in, and/or upregulated coincident with, *in vitro* biofilm formation by strain ES114 (Shibata and Visick, 2012, Ray *et al*., 2015), and could contribute to hyperaggregation in a *syp*-dependent manner.

Should such differences in regulation exist between the normal and hyperaggregating strains, it is possible that they are mediated by genes present in the additional 250 kb of genetic material found in the D-type strains (Bongrand *et al*., 2016); however, it should be noted that hyperaggregation can also result from over-expression of a single regulatory gene in a strain that does not carry the 250 kb (Yip *et al*., 2006). Such questions are the subject of an ongoing comparative study focused on the different biofilm regulatory cascades in the two strains.

The formation of aggregates on the light organ's surface is restricted to the Vibrionaceae

Although *V. fischeri* is the only species that can colonize the light organ in nature, and *V. fischeri* ES114 can exclude other species from aggregating on the organ's surface (Nyholm *et al*., 2000), when *V. fischeri* is absent, several marine bacteria will form a surface aggregation (Altura *et al*., 2013). We followed the development of such aggregates by confocal microscopy from 10 min to 6 h post-inoculation. Juvenile *E. scolopes* were inoculated with one of eight marine Gram-negative species (5 Vibrionaceae and 3 non-Vibrionaceae) or three marine Gram-positive species, and their behaviour compared with that of the squid symbiont *V. fischeri* ES114.

Consistent with previous reports (Nyholm and McFall-Ngai, 2003), even after 6 h, none of the Gram-positive strains had formed aggregations on the light organ (Table 2). This finding is surprising because biomechanical studies have shown that the light organ's metachronally beating long cilia efficiently entrain bacteria-sized plastic beads into the region of short cilia above the pores, where aggregates form (Nawroth *et al*., 2017). It is here that *V. fischeri* cells attach to the tips of the cilia, and from which they colonize host tissues. The failure of Gram-positive bacteria to aggregate in this region may reflect their high sensitivity to antimicrobials such as peptidoglycan-recognition protein and lysozyme that are present there (Troll *et al*., 2010; Kremer *et al*., 2013). Like the Gram-positive strains, none of the three non-Vibrionaceae marine Gram-negative species were observed to aggregate, even though two of them (*Pseudoalteromonas luteoviolacea* HI1 and *Leisingera* sp. ANG1) associate with marine invertebrates (Shikuma *et al*., 2014; Gromek *et al*., 2016).

In contrast, two of the Vibrionaceae strains, *V. campbellii* KNH1 and *Photobacterium leiognathi* KNH6, produced aggregates indistinguishable from *V. fischeri* ES114 (i.e., on average 35–40 cells, in over half of the animals observed) within 2 h of inoculation. The other three Vibrionaceae strains (*V. anguillarum* CAIM8, *V. nigripulchritudo* CAIM323T, and *V. campbellii* CAIM1436) formed only small (~ 3–10 cells) aggregates on the organ that took 4–6 h to develop (Table 2; Fig. 6). Interestingly, just as different strains of *V. fischeri* displayed a range of aggregation behaviour (Table 1), the two *V. campbellii* strains tested varied 100-fold in their level of aggregate formation. In summary, all these Vibrionaceae species were able to form surface associations; however, only *V. fischeri* could colonize the light organ. Thus, the ability to aggregate on the light-organ surface is a necessary, but not sufficient, step in initiating

Table 2. Aggregation characteristics of different bacterial phylotypes

Species[a] (strain)	Phylum (Gram ±)	Aggregates observed[b]	Average cells in an aggregate (range)[c]	Approximate time to form cells an aggregate (h)[d]
Vibrio fischeri (ES114)	γ-Proteo (−)	24/24	41 (1–200)	1
V. fischeri (MJ11)	γ-Proteo (−)	8/21	12 (4–33)	4
V. campbellii (KNH1)	γ-Proteo (−)	16/37	161 (6–1800)	1.5
V. campbellii (CAIM1436)	γ-Proteo (−)	1/27	3	5.5
V. anguillarum (CAIM8)	γ-Proteo (−)	4/26	6 (4–9)	5.5
V. nigripulchritudo (CAIM323T)	γ-Proteo (−)	4/22	6 (5–7)	4.5
Ph, leiognathi (KNH6)	γ-Proteo (−)	18/29	35 (3–120)	2
Ps. luteoviolacea (HI1)	γ-Proteo (−)	0/22	−	−
Leisingera sp. (ANG1)	α-Proteo (−)	0/21	−	−
Cellulophaga lytica	*Bacteroidetes* (−)	0/20	−	−
Bacillus algicola	*Firmicutes* (+)	0/18	−	−
B. aquimaris	*Firmicutes* (+)	0/22	−	−
Exiguobacterium aestuarii	*Firmicutes* (+)	0/13	−	−

[a]Species above the dashed line are *Vibrionaceae*; *Ph.* = *Photobacterium*; *Ps.* = *Pseudoalteromonas*.
[b]Number of animals with aggregates/total number observed; inoculated with 10^5 CFU/ml seawater.
[c]Approximate number of cells in the aggregate (see *Experimental procedures* for details).
[d]Time after inoculation at which the first evidence of aggregated cells was observed.

symbiosis. The finding that aggregation was restricted to the Vibrionaceae suggests a highly specific mechanism by which the host, after entraining bacteria-sized particles to the site of aggregation (Nawroth *et al*., 2017), must further discriminate among the Vibrionaceae to promote exclusive colonization by *V. fischeri*.

Conclusions

The present study characterizes the impact of species and strain differences on the first interactions of environmental bacteria with host tissues during the establishment of a natural symbiosis. Using the model squid–vibrio partnership, the data demonstrate that, while a small subset of environmental bacteria, that is, members of the family Vibrionaceae, will aggregate on host mucociliary surfaces, only strains of *V. fischeri* are capable of colonizing host tissues. Within *V. fischeri*, different strains vary dramatically in both aggregation behaviour and effect on host ciliated surfaces. Because these events are directly observable, and occur within minutes to hours, the data offer insight into how, under natural conditions, other mucociliary tissues might behave during their initial encounter with bacteria. While it will be difficult to apply this approach to the inaccessible mucociliary membranes of mammalian systems, such as the trachea and fallopian tubes, the results presented here promise to provide heuristic value for the design, modelling and experimentation of ciliated tissues in organ culture (Whitaker *et al*., 2017).

Experimental procedures

General

Adult Hawaiian bobtail squid, *Euprymna scolopes*, were caught in Maunalua Bay, Oahu, Hawai'i as previously described (Doino and McFall-Ngai, 1995) and maintained in a flow-through ocean seawater system at the Kewalo Marine Laboratory. Egg clutches laid in the system by female adults were transferred into smaller aquaria containing seawater free of *V. fischeri*, where they were incubated at 20°C (±2°C). After hatching, the juvenile squid for all experiments were collected and transferred to UV-sterilized seawater prior to treatments and inoculations.

All chemicals were purchased from Sigma-Aldrich (St. Louis, MI) or Thermo Fisher Scientific (Waltham, MA), unless otherwise stated. Restriction enzymes were purchased at New England BioLabs (Ipswich, MA).

Bacterial culture conditions

To initiate animal inoculations, all bacterial strains (Table 1) were recovered from glycerol stocks by spreading on a rich-medium (LBS) agar, and then grown overnight in LBS broth at 28°C. LBS medium consists of 20 g NaCl, 50 ml of 1 M Tris–HCl (pH 7.5), 10 g Bacto-Tryptone and 5 g yeast extract per litre (Graf *et al*., 1994; Stabb *et al*., 2001). For green fluorescent protein (GFP)- and red fluorescent protein (RFP)-labelled bacterial strains, 100 μg of kanamycin (Kn) or 2.5 μg of chloramphenicol (Cm), respectively, were added per ml of the
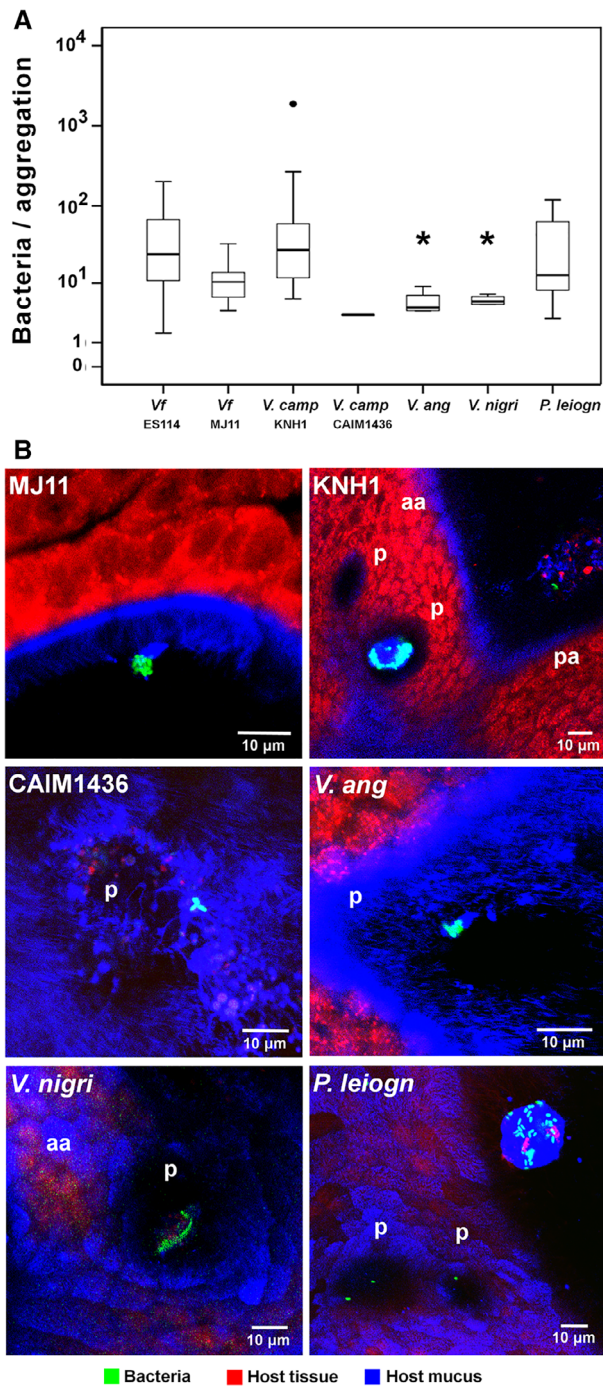
Fig. 6. Aggregation behaviour of environmental bacteria. A. Sizes of aggregates of bacterial species that have the ability to form aggregations on the light organ surface at inocula of 10^5 CFU ml^{-1} (Kruskal–Wallis Test: Chi^2 = 18.623, df = 6, p = 0.005); bold horizontal lines represent medians; boxes comprise the interquartile ranges; bars indicate the 1.5IQR of the data shown; dots represent outliers; asterisks indicate a significant difference in comparison to the control, S-type strain *V. fischeri* ES114 (*V. anguillarum*: Mann–Whitney U = 10.0, Wilcoxon W = 20.0, Z = −2.324, p = 0.018; *V. nigripulchritudo*: Mann–Whitney U = 9.0, Wilcoxon W = 19.0, Z = −2.402, p = 0.013). B. Laser scanning-confocal micrographs show differences between the aggregation on the light-organ surface of *V. fischeri* and other environmental bacteria; aa, anterior appendage; p, posterior appendage; p, pores. Environmental

overnight culture to ensure selection for cells carrying the plasmid-borne fluorescent protein (Supporting Information Table S2) (Dunn *et al.*, 2006). Other antibiotics, at the indicated final concentrations: Cm, erythromycin (Em), or tetracycline (Tc) were added to growth media as necessary at 1, 2.5 or 5 μg ml^{-1} respectively.

Escherichia coli DH5α was grown at 37°C in LB medium (Davis *et al.*, 1980) containing 10 g Bacto-Tryptone, 5 g yeast extract and 10 g NaCl per litre. As necessary, antibiotics were added to growth media at the indicated final concentrations: Kn, Cm or Tc, at 50, 12.5 or 15 μg ml^{-1}. Solid media were made using agar at a final concentration of 1.5%. Thymidine (0.3 mM) was added to media for growth of *E. coli* strain π3813.

For aggregation experiments, overnight cultures of marine bacteria were sub-cultured in a 1:100 dilution in seawater tryptone medium (SWT), containing 700 ml seawater, 300 ml deionized water, 5 g Bacto-Tryptone, 3 g yeast extract and 3 ml of glycerol per litre (Boettcher and Ruby 1990). Bacteria were grown to mid-exponential phase (OD$_{600}$ ~ 0.3–0.6) with shaking before diluting them in seawater. Imaging of bacterial strains not genetically modified to carry GFP, was achieved by staining with 150 μl of ATTO495 fluorescent dye (0.5 mg/ml; AttoTec, Germany) in 3 ml of SWT medium, followed by approximately 2 h of bacterial growth in darkness, using the protocol described previously (Soto-Rodriguez *et al.*, 2003).

Strain verification

16S amplicon sequencing was used to verify the identity of the environmental bacterial strains used in this study. Individual bacterial strains were grown in liquid culture and an aliquot was then centrifuged to pellet the bacteria. The supernatant was removed and the pellet used for nucleic acid extraction using the Epicentre MasterPure™ DNA extraction kit (Epicentre Technologies, Madison, WI). Finally, the DNA pellet was resuspended in 50 μl RNase-free low-TE buffer (1 mM Tris–HCl at pH 8.0, and 0.01 mM EDTA), and stored at −80°C.

PCR with the general eubacterial primer pair fD1 and rP2 (Weisburg *et al.*, 1991) amplified the 16S gene of each DNA sample. Amplification was performed on a BioRad C1000 Touch Thermocycler in a total reaction volume of 12.5 μl, containing 1 μl template DNA, 2.5 μl 5X GoTaq® Reaction Buffer (pH 8.5), 1.5 mM MgCl$_2$, 0.2 mM dNTPs, 0.5 μM of each primer and 0.25 U GoTaq® DNA-Polymerase (Promega, Madison, WI).

phylotypes (Supporting Information Table S1): *V. camp*, *Vibrio campbellii*; *V. ang*, *Vibrio anguillarum*; *V. nigri*, *V. nigripulchritudo*; *P. leiogn*, *Photobacterium leiognathi*. Red, Cell Tracker Orange; blue, WGA (wheat-germ agglutinin) Alexa 633. [Color figure can be viewed at wileyonlinelibrary.com]

Cycle parameters were as follows: an initial denaturation step at 95°C for 2 min, 35 cycles of 95°C for 60 s, 65°C for 60 s and 72°C for 90 s, and a final extension step of 72°C for 5 min. PCR success was verified by gel electrophoresis using a GelRed™ (Biotium, Fremont, CA) stained 1.5% TAE agarose gel (150 V, 20 min). The documentation of gel pictures was conducted using ChemiDoc-It[2] Imager and the UVP VisionWorksLS software, version 8.6.15114.8618 (UVP®, Upland, CA). Positive bands were excised from the gel and purified using Wizard® SV Gel and PCR clean-up system (Promega, Madison, WI). The final DNA concentration of the purified PCR product was obtained from NanoDrop measurments (ND2000 photo-spectrometer). Sequencing was performed commercially at Genewiz® (South Plainfield, NJ).

Bacterial strains and mutant construction

The following *E. coli* strains were used for the purposes of cloning, plasmid maintenance, and conjugation: TAM1 (Active Motif, Carlsbad, CA, USA), DH5α and π3813 (Le Roux *et al*., 2007) (Table 1). Derivatives of *V. fischeri* were generated either by conjugation (DeLoney *et al*., 2002) or by natural transformation (Pollack-Berti *et al*., 2010; Brooks *et al*., 2014). Using the conjugation-based approach, an *rscS* deletion mutation was constructed in the D-type strain MB13B2 as described previously (Stabb and Ruby, 2002; Le Roux *et al*., 2007) with one modification. To build the recombinant plasmid, we first PCR amplified two fragments of *V. fischeri* MB13B2 DNA using primers 41 and 42, or primers 43 and 44 (Supporting Information Table S3). The two products were digested with SphI, and ligated together with T4 DNA ligase. The resulting sequence was amplified with primers 41 and 44. This PCR product, and the mobilizable suicide vector pKV363 (Shibata and Visick, 2012), were digested with SalI and XhoI and ligated together. The resulting plasmid was conjugated into MB13B2, and recombinants with a deletion of *rscS* were obtained.

For the transformation approach, PCR SOEing (splicing by overlap extension) (Ho *et al*., 1989) reactions were performed using EMD Millipore Novagen KOD high fidelity polymerase, and Promega Taq was used to confirm gene replacement events. Marked deletions of *sypQ* were generated by PCR SOEing using the primers listed in Supporting Information Table S3. Sequences (~ 500 bp) upstream (primers 1188 and 2174) and downstream (2175 and 443) of the target gene were amplified by PCR, then fused with an Em[R] antibiotic-resistance cassette (primers 2089 and 2090) in a PCR SOEing reaction. The final spliced PCR product was introduced into a *tfoX*-overexpressing ES114 strain carrying pLosTfoX-Kan (Brooks *et al*., 2014) by natural transformation (Pollack-Berti *et al*., 2010). Recombination of the PCR product into the chromosome resulted in the desired gene-replacement mutant, which was selected using the Em[R] marker. Chromosomal DNA was isolated from recombinants of *V. fischeri* strain ES114 using the DNeasy Blood & Tissue Kit (Qiagen, Germantown, MD) and used to introduce the desired mutation into *tfoX*-overexpressing MB13B2 cells.

Imaging of bacterial aggregations

To assess bacterial aggregation during symbiosis initiation, juvenile squid were incubated for between 10 min to 6 h in seawater containing 10^5 CFU/ml (unless stated otherwise) of either *V. fischeri* strains, or other Gram-negative and -positive marine bacteria (Tables 1 and 2). The animals were then stained with different fluorescent dyes such as Cell Tracker Orange (1:10^4) and wheat-germ agglutinin WGA Alexa Fluor 633 (1:40) (Thermo Fisher Scientific, Inc.) for 1–5 min, which labels host tissues and mucus respectively. Bacterial strains were detected using either a GFP label (carried on pVSV102), or the ATTO495 fluorescent dye, which was used to label with *V. nigripulchritudo* CAIM323T as it was resistant to the triparental mating protocol for acquisition of the plasmid. Animals were anaesthetised in 2% ethanol (EtOH), the mantle and funnel were removed to allow for visualization of the organ, and bacterial aggregation behaviour on the organ surface was monitored at intermittent time points between 10 min and 6 h post-inoculation using a Zeiss LSM710 laser-scanning confocal microscope (Carl Zeiss Microscopy, Jena, Germany).

For the comparison of aggregation differences between the D- and S-type *V. fischeri* strains (Bongrand *et al*., 2016), squid were treated as described above with the following modification: animals were anaesthetised in 2% EtOH after inoculation with bacteria, and subsequently fixed in 4% paraformaldehyde for 2 days. After fixation, the juvenile squid were rinsed four times, for 10–15 min, in 1× mPBS (marine phosphate buffered saline—50 mM sodium phosphate, 0.45 M NaCl, pH 7.4) and were then fluorescently stained using the TOTO-3 fluorescent dye (Thermo Fisher Scientific, Inc.) at 1:650 in 1% Triton-X100 in mPBS for 1–2 h. After staining, samples were again rinsed two times in Triton X100-mPBS for 10–15 min, followed by two rinses of 10–15 min in 1× mPBS. These two different methods (the observation of live specimens, as well as samples that were fixed in 4% paraformaldehyde) allowed us to define the earliest time of bacterial aggregation, and to standardize the specific time point for aggregate-size measurement respectively.

Estimation of aggregate size

The size of bacterial aggregates, as observed by laser-scanning confocal microscopy, was compared among

strains to identify differences in the extent of bacterial aggregation. Two different methods were applied using the particle analysis tool of the FIJI-ImageJ imaging software (fiji.sc) to calculate spatial measurements based on fluorescence intensity. For fixed samples, a Z-stack was acquired using the LSM710 confocal microscope. Subsequently, multiple images in the Z-stack of one sample were projected onto one plane and the area (in μm^2) of green (i.e., GFP) fluorescence was calculated, with 2 μm^2 as the minimum threshold for bacterial size. Based on the acquired area, and the assumption of a bacterial cell cross-section being approximately 2 μm^2, we estimated the number of cells present in a bacterial aggregation. All statistical analyses were performed using SPSS 25.0 Software (IBM, New York, NY).

Interaction of D-type V. fischeri with light-organ cilia

To visualize the interaction of bacteria adhering to cilia on the organ surface, juvenile squid were exposed to 250 nM Tubulin Tracker in seawater after incubation with GFP- and RFP-labelled bacteria (Altura *et al.*, 2013). Aposymbiotic animals were treated filtered seawater as a negative control. Subsequently, the animal tissues were fluorescently labelled as described above for observation by laser-scanning confocal microscope.

The density of interactions in aggregations of *V. fischeri* MB13B2 it made possible to locate and examine the ultrastructure of the paddle-like ciliary ends. For this transmission electron microscopy (TEM), we incubated juvenile squid with the *V. fischeri* MB13B2 for 30 min, anaesthetised the animals with 2% EtOH, and then transferred them into fixative (2% paraformaldehyde and 2% glutaraldehyde in 1× mPBS) for 48 h at 4°C. We then rinsed the samples two times for 15 min with 1× mPBS. For post-fixation, we incubated the samples with 1% osmium tetroxide in 0.1 M cacodylate buffer (pH 7.4) for 1 h, followed by two rinses of 10 min each with 1× mPBS. The samples were dehydrated in a graded EtOH series and embedded in Spurr's resin. Ultrathin (60–80 nm) sections were obtained on a Powertome ultramicrotome (RMC Boeckeler, Tucson, AZ), double stained with uranyl acetate (2% in distilled water) and lead citrate (Reynolds, 1963), and viewed on a Hitachi HT7700 TEM at 100 kV.

Biofilm assays

To assess wrinkled-colony formation, *V. fischeri* strains were subcultured in 5 ml of LBS medium at 28°C. Following growth to early-log phase, the cultures were standardized to an optical density at 600 nm (OD_{600}) of 0.2. LBS agar plates were spotted with 10 µl aliquots, and incubated at 24°C. Images of the spotted cultures were acquired over the course of wrinkled-colony formation at the indicated times using a Zeiss Stemi 2000-C dissecting microscope. At the end of the time course, the colonies were disrupted with a toothpick to assess colony cohesiveness, which is an indicator of the extent of Syp polysaccharide production (Ray *et al.*, 2015).

Pellicle formation was visualized in *V. fischeri* strains grown overnight and subcultured in LBS with shaking. Following growth to mid-log phase, the cultures were allowed to stand statically at 24°C for 10 days. Cultures were gently perturbed prior to imaging with an iPhone 7 camera.

References

Aanen, D.K., Eggleton, P., Rouland-Lefevre, C., Guldberg-Froslev, T., Rosendahl, S., and Boomsma, J.J. (2002) The evolution of fungus-growing termites and their mutualistic fungal symbionts. *Proc Natl Acad Sci USA* **99**: 14887–14892.

Altura, M.A., Heath-Heckman, E.A., Gillette, A., Kremer, N., Krachler, A.M., Brennan, C., *et al*. (2013) The first engagement of partners in the *Euprymna scolopes*-*Vibrio fischeri* symbiosis is a two-step process initiated by a few environmental symbiont cells. *Environ Microbiol* **15**: 2937–2950.

Bastone, R.T., Dutton, E.M., Wang, D., Yang, M., and Frederickson, M.E. (2017) The evolution of symbiont preference traits in the model legume *Medicago truncatula*. *New Phytol* **213**: 1850–1861.

Boettcher, K.J., and Ruby, E.G. (1990) Depressed light emission by symbiotic *Vibrio fischeri* of the sepiolid squid *Euprymna scolopes*. *J Bacteriol* **172**: 3701–3706.

Bongrand, C., Koch, E.J., Moriano-Gutierrez, S., Cordero, O. X., McFall-Ngai, M., Polz, M.F., and Ruby, E.G. (2016) A genomic comparison of 13 symbiotic *Vibrio fischeri* isolates from the perspective of their host source and colonization behavior. *ISME J* **10**: 2907–2917.

Bright, M., and Bulgheresi, S. (2010) A complex journey: transmission of microbial symbionts. *Nat Rev Microbiol* **8**: 218–230.

Brooks, J.F., 2nd, Gyllborg, M.C., Cronin, D.C., Quillin, S.J., Mallama, C.A., *et al*. (2014) Global discovery of colonization determinants in the squid symbiont *Vibrio fischeri*. *Proc Natl Acad Sci USA* **111**: 17284–17289.

Brooks, J.F., 2nd, and Mandel, M.J. (2016) The histidine kinase BinK is a negative regulator of biofilm formation and squid colonization. *J Bacteriol* **198**: 2596–2607.

Cao, M., and Goodrich-Blair, H. (2017) Ready or not: microbial adaptive responses in dynamic symbiosis environments. *J Bacteriol* **199**: e00883–e00816.

Caro-Quintero, A., and Ochman, H. (2015) Assessing the unseen bacterial diversity in microbial communities. *Genome Biol Evol* **7**: 3416–3425.

Davis, R.W., Botstein, D., and Roth, J.R. (1980) *Advanced Bacterial Genetics*. Cold Spring Harbor, NY: Cold Spring Harbor Laboratory.

Deiner, M., Tamm, S.L., and Tamm, S. (1993) Mechanical properties of ciliary axonemes and membranes as shown by paddle cilia. *J Cell Sci* **104**: 1251–1262.

Deines, P., Lachnit, T., and Bosch, T.C.G. (2017) Competing forces maintain the *Hydra* metaorganism. *Immunol Rev* **279**: 123–136.

DeLoney, C.R., Bartley, T.M., and Visick, K.L. (2002) Role for phosphoglucomutase in *Vibrio fischeri-Euprymna scolopes* symbiosis. *J Bacteriol* **184**: 5121–5129.

Doino, J.A., and McFall-Ngai, M.J. (1995) A transient exposure to symbiosis-competent bacteria induces light organ morphogenesis in the host squid. *Biol Bull* **189**: 347–355.

Dunn, A.K., Millikan, D.S., Adin, D.M., Bose, J.L., and Stabb, E.V. (2006) New rfp- and pES213-derived tools for analyzing symbiotic *Vibrio fischeri* reveal patterns of infection and *lux* expression in situ. *Appl Environ Microbiol* **72**: 802–810.

Ellegaard, K.M., and Engel, P. (2016) Beyond 16S rRNA community profiling: intra-species diversity in the gut microbiota. *Front Microbiol* **7**: 1475.

Ezzakkioui, F., El Mourabit, N., Chahboune, R., Castellano-Hinojosa, A., Bedmar, E.J., and Barrijal, S. (2015) Phenotypic and genetic characterization of rhizobia isolated from *Hedysarum flexuosum* in northwest region of Morocco. *J Basic Microbiol* **55**: 830–837.

Frank, S.A. (1996) Host-symbiont conflict over the mixing of symbiotic lineages. *Proc Biol Sci* **263**: 339–344.

Goodrich-Blair, H. (2007) They've got a ticket to ride: *Xenorhabdus nematophila-Steinernema carpocapsae* symbiosis. *Curr Opin Microbiol* **10**: 225–230.

Graf, J., Dunlap, P.V., and Ruby, E.G. (1994) Effect of transposon-induced motility mutations on colonization of the host light organ by *Vibrio fischeri*. *J Bacteriol* **176**: 6986–6991.

Graf, J., Kikuchi, Y., and Rio, R.V. (2006) Leeches and their microbiota: naturally simple symbiosis models. *Trends Microbiol* **14**: 365–371.

Greenblum, S., Carr, R., and Borenstein, E. (2015) Extensive strain-level copy-number variation across human gut microbiome species. *Cell* **160**: 583–594.

Gromek, S.M., Suria, A.M., Fullmer, M.S., Garcia, J.L., Gogarten, J.P., et al. (2016) *Leisingera* sp. JC1, a bacterial isolate from Hawaiian bobtail squid eggs, produces indigoidine and differentially inhibits vibrios. *Front Microbiol* **7**: 1342.

Heath, K.D., and Tiffin, P. (2007) Context dependence in the coevolution of plant and rhizobial mutualists. *Proc Biol Sci* **274**: 1905–1912.

Ho, S.N., Hunt, H.D., Horton, R.M., Pullen, J.K., and Pease, L.R. (1989) Site-directed mutagenesis by overlap extension using the polymerase chain reaction. *Gene* **77**: 51–59.

Jones, B.W., Maruyama, A., Ouverney, C.C., and Nishiguchi, M.K. (2007) Spatial and temporal distribution of the Vibrionaceae in coastal waters of Hawaii, Australia, and France. *Microb Ecol* **54**: 314–323.

Kiers, E.T., Rousseau, R.A., West, S.A., and Denison, R.F. (2003) Host sanctions and the legume-*Rhizobium* mutualism. *Nature* **425**: 78–81.

Kremer, N., Philipp, E.E., Carpentier, M.C., Brennan, C.A., Kraemer, L., et al. (2013) Initial symbiont contact orchestrates host-organ-wide transcriptional changes that prime tissue colonization. *Cell Host Microbe* **14**: 183–194.

Kwong, W.K., and Moran, N.A. (2016) Gut microbial communities of social bees. *Nat Rev Microbiol* **14**: 374–384.

Le Roux, F., Binesse, J., Saulnier, D., and Mazel, D. (2007) Construction of a *Vibrio splendidus* mutant lacking the metalloprotease gene *vsm* by use of a novel counterselectable suicide vector. *Appl Environ Microbiol* **73**: 777–784.

Mandel, M.J., Wollenberg, M.S., Stabb, E.V., Visick, K.L., and Ruby, E.G. (2009) A single regulatory gene is sufficient to alter bacterial host range. *Nature* **458**: 215–218.

Marsden, A.E., Grudzinski, K., Ondrey, J.M., DeLoney-Marino, C.R., and Visick, K.L. (2017) Impact of salt and nutrient content on biofilm formation by *Vibrio fischeri*. *PLoS One* **12**: e0169521.

McFall-Ngai, M.J. (1998) The development of cooperative associations between animals and bacteria: establishing detente among domains. *Am Zool* **38**: 593–608.

McFall-Ngai, M.J. (2014) The importance of microbes in animal development: lessons from the squid-vibrio symbiosis. *Annu Rev Microbiol* **68**: 177–194.

McFall-Ngai, M.J., and Ruby, E.G. (1991) Symbiont recognition and subsequent morphogenesis as early events in an animal-bacterial mutualism. *Science* **254**: 1491–1494.

McFall-Ngai, M., Nyholm, S.V., and Castillo, M.G. (2010) The role of the immune system in the initiation and persistence of the *Euprymna scolopes--Vibrio fischeri* symbiosis. *Semin Immunol* **22**: 48–53.

McMullen, J.G., 2nd, Peterson, B.F., Forst, S., Blair, H.G., and Stock, S.P. (2017) Fitness costs of symbiont switching using entomopathogenic nematodes as a model. *BMC Evol Biol* **17**: 100.

Mueller, N.T., Bakacs, E., Combellick, J., Grigoryan, Z., and Dominguez-Bello, M.G. (2015) The infant microbiome development: mom matters. *Trends Mol Med* **21**: 109–117.

Murfin, K.E., Lee, M.M., Klassen, J.L., McDonald, B.R., Larget, B., et al. (2015) *Xenorhabdus bovienii* strain diversity impacts coevolution and symbiotic maintenance with *Steinernema* spp nematode hosts. *mBio* **6**: e00076.

Nawroth, J.C., Guo, H., Koch, E., Heath-Heckman, E.A.C., Hermanson, J.C., Ruby, E.G., et al. (2017) Motile cilia create fluid-mechanical microhabitats for the active recruitment of the host microbiome. *Proc Natl Acad Sci USA* **114**: 9510–9516.

Noecker, C., McNally, C.P., Eng, A., and Borenstein, E. (2017) High-resolution characterization of the human microbiome. *Transl Res* **179**: 7–23.

Norsworthy, A.N., and Visick, K.L. (2015) Signaling between two interacting sensor kinases promotes biofilms and

colonization by a bacterial symbiont. *Mol Microbiol* **96**: 233–248.

Nyholm, S.V., and McFall-Ngai, M.J. (2003) Dominance of *Vibrio fischeri* in secreted mucus outside the light organ of *Euprymna scolopes*: the first site of symbiont specificity. *Appl Environ Microbiol* **69**: 3932–3937.

Nyholm, S.V., and McFall-Ngai, M.J. (2004) The winnowing: establishing the squid-vibrio symbiosis. *Nat Rev Microbiol* **2**: 632–642.

Nyholm, S.V., Stabb, E.V., Ruby, E.G., and McFall-Ngai, M.J. (2000) Establishment of an animal-bacterial association: recruiting symbiotic vibrios from the environment. *Proc Natl Acad Sci USA* **97**: 10231–10235.

Nyholm, S.V., Deplancke, B., Gaskins, H.R., Apicella, M.A., and McFall-Ngai, M.J. (2002) Roles of *Vibrio fischeri* and nonsymbiotic bacteria in the dynamics of mucus secretion during symbiont colonization of the *Euprymna scolopes* light organ. *Appl Environ Microbiol* **68**: 5113–5122.

Palmer, G.H., and Brayton, K.A. (2013) Antigenic variation and transmission fitness as drivers of bacterial strain structure. *Cell Microbiol* **15**: 1969–1975.

Pellmyr, O., and Huth, C.J. (1994) Evolutionary stability of mutualism between yuccas and yucca moths. *Nature* **372**: 257–260.

Pollack-Berti, A., Wollenberg, M.S., and Ruby, E.G. (2010) Natural transformation of *Vibrio fischeri* requires *tfoX* and *tfoY*. *Environ Microbiol* **12**: 2302–2311.

Poulsen, M., and Boomsma, J.J. (2005) Mutualistic fungi control crop diversity in fungus-growing ants. *Science* **307**: 741–744.

Powell, E., Ratnayeke, N., and Moran, N.A. (2016) Strain diversity and host specificity in a specialized gut symbiont of honeybees and bumblebees. *Mol Ecol* **25**: 4461–4471.

Ray, V.A., Driks, A., and Visick, K.L. (2015) Identification of a novel matrix protein that promotes biofilm maturation in *Vibrio fischeri*. *J Bacteriol* **197**: 518–528.

Reynolds, E.S. (1963) The use of lead citrate at high pH as an electron-opaque stain in electron microscopy. *J Cell Biol* **17**: 208–212.

Ruby, E.G., and Asato, L.M. (1993) Growth and flagellation of *Vibrio fischeri* during initiation of the sepiolid squid light organ symbiosis. *Arch Microbiol* **159**: 160–167.

Sachs, J.L., Mueller, U.G., Wilcox, T.P., and Bull, J.J. (2004) The evolution of cooperation. *Q Rev Biol* **79**: 135–160.

Salem, H., Florez, L., Gerardo, N., and Kaltenpoth, M. (2015) An out-of-body experience: the extracellular dimension for the transmission of mutualistic bacteria in insects. *Proc Biol Sci* **282**: 20142957.

Shibata, S., and Visick, K.L. (2012) Sensor kinase RscS induces the production of antigenically distinct outer membrane vesicles that depend on the symbiosis polysaccharide locus in *Vibrio fischeri*. *J Bacteriol* **194**: 185–194.

Shibata, S., Yip, E.S., Quirke, K.P., Ondrey, J.M., and Visick, K.L. (2012) Roles of the structural symbiosis polysaccharide (*syp*) genes in host colonization, biofilm formation, and polysaccharide biosynthesis in *Vibrio fischeri*. *J Bacteriol* **194**: 6736–6747.

Shikuma, N.J., Pilhofer, M., Weiss, G.L., Hadfield, M.G., Jensen, G.J., and Newman, D.K. (2014) Marine tubeworm metamorphosis induced by arrays of bacterial phage tail-like structures. *Science* **343**: 529–533.

Short, G., and Tamm, S.L. (1991) On the nature of paddle cilia and discocilia. *Biol Bull* **180**: 466–474.

Siller, S.S., Burke, M.C., Li, F.Q., and Takemaru, K. (2015) Chibby functions to preserve normal ciliary morphology through the regulation of intraflagellar transport in airway ciliated cells. *Cell Cycle* **14**: 3163–3172.

Soto-Rodriguez, S.A., Simoes, N., Jones, D.A., Roque, A., and Gomez-Gil, B. (2003) Assessment of fluorescent-labeled bacteria for evaluation of *in vivo* uptake of bacteria (*Vibrio* spp.) by crustacean larvae. *J Microbiol Methods* **52**: 101–114.

Stabb, E.V., and Ruby, E.G. (2002) RP4-based plasmids for conjugation between *Escherichia coli* and members of the Vibrionaceae. *Methods Enzymol* **358**: 413–426.

Stabb, E.V., Reich, K.A., and Ruby, E.G. (2001) *Vibrio fischeri* genes *hvnA* and *hvnB* encode secreted NAD (+)-glycohydrolases. *J Bacteriol* **183**: 309–317.

Takashita, K., and Kikuchi, Y. (2017) *Riptortus pedestria* and *Burkholderia* symbiont: an ideal model system for insect-microbe symbiotic associations. *Res Microbiol* **168**: 175–187.

Tischler, A.H., Lie, L., Thompson, C.M., and Visick, K.L. (2018) Discovery of calcium as a biofilm-promoting signal for *Vibrio fischeri* reveals new phenotypes and underlying regulatory complexity. *J Bacteriol* **200**: e00016–e00018.

Troll, J.V., Bent, E.H., Pacquette, N., Wier, A.M., Goldman, W.E., Goldman, W.E., *et al*. (2010) Taming the symbiont for coexistence: a host PGRP neutralizes a bacterial symbiont toxin. *Environ Microbiol* **12**: 2190–2203.

Visick, K.L. (2009) An intricate network of regulators controls biofilm formation and colonization by *Vibrio fischeri*. *Mol Microbiol* **74**: 782–789.

Visick, K.L., and Skoufos, L.M. (2001) Two-component sensor required for normal symbiotic colonization of *Euprymna scolopes* by *Vibrio fischeri*. *J Bacteriol* **183**: 835–842.

Wang, Y., Dunn, A.K., Wilneff, J., McFall-Ngai, M.J., Spiro, S., and Ruby, E.G. (2010) *Vibrio fischeri* flavohaemoglobin protects against nitric oxide during initiation of the squid-*Vibrio* symbiosis. *Mol Microbiol* **78**: 903–915.

Weisburg, W.G., Barns, S.M., Pelletier, D.A., and Lane, D.J. (1991) 16S ribosomal DNA amplification for phylogenetic study. *J Bacteriol* **173**: 697–703.

Whitaker, W.R., Shepherd, E.S., and Sonnenburg, J.L. (2017) Tunable expression tools enable single-cell strain distinction in the gut microbiome. *Cell* **169**: 538–546.

Wollenberg, M.S., and Ruby, E.G. (2009) Population structure of *Vibrio fischeri* within the light organs of *Euprymna scolopes* squid from two Oahu (Hawaii) populations. *Appl Environ Microbiol* **75**: 193–202.

Wollenberg, M.S., and Ruby, E.G. (2012) Phylogeny and fitness of *Vibrio fischeri* from the light organs of *Euprymna scolopes* in two Oahu, Hawaii populations. *ISME J* **6**: 352–362.

Yip, E.S., Grublesky, B.T., Hussa, E.A., and Visick, K.L. (2005) A novel, conserved cluster of genes promotes symbiotic colonization and sigma-dependent biofilm formation by *Vibrio fischeri*. *Mol Microbiol* **57**: 1485–1498.

Yip, E.S., Geszvain, K., DeLoney-Marino, C.R., and Visick, K.L. (2006) The symbiosis regulator RscS controls the syp gene locus, biofilm formation and symbiotic aggregation by *Vibrio fischeri*. *Mol Microbiol* **62**: 1586–1600.

Supporting Information